Internal mechanical dissipation mechanisms in amorphous silicon

Carl Lévesque,[*] Sjoerd Roorda ,[†] François Schiettekatte ,[‡] and Normand Mousseau [§]

Département de Physique and Regroupement québécois sur les matériaux de pointe, Université de Montréal, C.P. 6128, Succursale Centre-Ville, Montréal, Québec, Canada H3C 3J7

Using activation-relaxation technique nouveau (ARTN), we search for two-level systems (TLSs) in models of amorphous silicon (*a*-Si). The TLSs are mechanisms related to internal mechanical dissipation and represent the main source of noise in the most sensitive frequency range of the largest gravitational wave detectors as well as one of the main sources of decoherence in many quantum computers. We show that in *a*-Si, the majority of the TLSs of interest fall into two main categories: bond-defect hopping, where neighbors exchange a topological defect, and Wooten-Winer-Weaire bond exchange. The distribution of these categories depends heavily on the preparation schedule of the *a*-Si. We use our results to compute the mechanical loss in amorphous silicon, leading to a loss angle of 10^{-3} at room temperature, decreasing to 10^{-4} at 150 K in some configurations. Our modeling results indicate that multiple classes of events can cause experimentally relevant TLSs in disordered materials and therefore multiple attenuation strategies might be needed to reduce their impact.

I. INTRODUCTION

Current gravitational wave detectors (GWDs) consist of Michelson interferometers with arms the length of a few kilometers containing a Fabry-Perot cavity. Since 2015 [1], GWDs have successfully detected nearly a hundred events [2], at an accelerating pace thanks to continuous efforts. Among the targets for improvement are the test masses: massive dielectric mirrors at the end of each arm. Their reflective surfaces consist of a stack of alternating high-refractive-index (HR) and low-refractive-index (LR) materials. In the current implementation of LIGO and Virgo, the LR material for coating is amorphous silica, and the HR material is Ti-doped amorphous tantala [3]. Amorphous materials, especially in the HR layers, present intrinsic fluctuations that can be directly linked to the mechanical dissipation (Q^{-1}) and thermal noise through the fluctuation-dissipation theorem [4–6]. Such phenomena also cause decoherence in some quantum computers [7]. Despite considerable efforts to reduce these losses in the HR layers [8–10], low mechanical loss remains the limiting factor of noise at frequencies around 50 Hz in major GWDs, at which these detectors are the most sensitive [11].

Here, we investigate the origin of the mechanisms leading to internal mechanical dissipation through atomistic simulations, by finding two-level systems (TLSs). We conduct over 6 000 000 event searches for TLSs in 201 amorphous solid configurations. This leads to the identification of 423 TLSs.

In order to simplify the problem, we investigate amorphous silicon (*a*-Si), a prototypical model of a continuous random network. *a*-Si consists of a single element, and its structure

and dynamics have been under investigation for more than 50 years [12]. Beyond its generic interest, *a*-Si is directly relevant in the GWD context as it is considered for future generations of GWDs [13]: It features a high refractive index, reducing the number of layers in the stack, and it can be synthesized with an ultralow internal mechanical dissipation [14].

We show that (i) TLSs are distributed within the experimentally relevant energy and frequency range; (ii) depending on the relaxation state of the material, relevant events are dominated by a dangling bond hop or the more elaborated Wooten-Winer-Weaire (WWW) [15] bond-exchange mechanism; and (iii) the loss angle deduced from our models is compatible with experiments. Overall, these results suggest that since multiple classes of events can be associated with TLSs in the same frequency range in disordered materials, multiple strategies might be needed to reduce their number.

II. THEORY AND METHODS

A. Two-level systems

Due to metastability associated with structural disorder and a distribution in local strain, amorphous materials present, intrinsically, more possibilities for the presence of local minima separated by low-energy barriers than their crystalline counterparts. As they evolve over time, solid-state systems can be pictured as transiting from one local minimum to the other in a potential energy landscape [16]. In the context of amorphous solids, a two-level system happens when two minima are connected by a low-energy single saddle point and surrounded by much higher energy barriers so that the system is locally trapped in a two-state basin.

Two-level systems (TLSs) in amorphous solids were first introduced as a way to explain the behavior of their specific heat and thermal conductivity at low temperatures [17]. Atoms tunneling through saddle points of TLSs provide more

---

[*]carl.levesque@umontreal.ca

[†]sjoerd.roorda@umontreal.ca

[‡]francois.schiettekatte@umontreal.ca
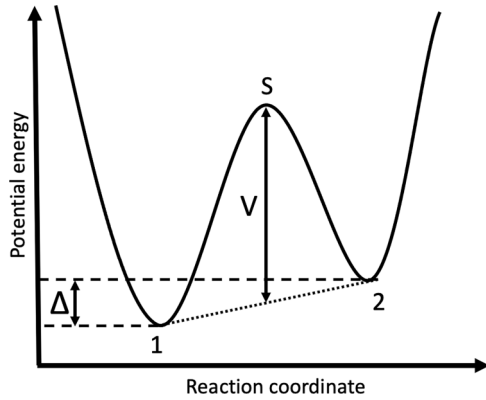
[§]normand.mousseau@umontreal.ca

FIG. 1. Potential energy landscape representation of a two-level system. Minima 1 and 2 are connected by a saddle point, point S. The mean barrier is V, and the asymmetry is Δ.

degrees of freedom to the system, increasing its heat capacity. As illustrated in Fig. 1, a TLS can be characterized by the energy of its saddle point (point S) relative to the minima (states 1 and 2), called the barrier (V), and the difference in energy between the two minima, called the asymmetry (Δ).

We note that while the rugged nature of the energy landscape of amorphous solids gives a very large, quasicontinuous global distribution of barriers and asymmetries [18], events are localized in space and distributed throughout all of the sample. Therefore they can be trapped by important gaps in the local barrier distributions, making dissipation a local phenomenon.

Assuming that quantum tunneling is negligible and that the system has time to thermalize in a local state after crossing a saddle point, the mean rate at which it will transition from minimum 1 to minimum 2, τ_{12}, is given by the Arrhenius law

$$\tau_{12} = \tau_0 e^{\frac{E_S - E_1}{k_B T}}, \qquad (1)$$

where τ_0^{-1} is the attempt frequency and E_s and E_1 are the energy levels at the saddle point and the first minimum, respectively. While attempt frequencies can vary considerably [19], calculations of these quantities in a-Si with the harmonic transition state theory were found to be close to 10^{13} s^{-1} with small fluctuations (see Fig. 9 in Ref. [20]). To shorten the simulations, we shall use a constant value of $\tau_0 = 10^{-13}$ s.

Because of the finite asymmetry Δ, τ_{12} is different from τ_{21}. For the whole TLS, a relaxation time τ is defined as a function of temperature T, V, Δ, and τ_0 [21]

$$\tau = \tau_0 \operatorname{sech}\left(\frac{\Delta}{2k_B T}\right) e^{\frac{V}{k_B T}}. \qquad (2)$$

Mechanical dissipation in the frequency regime of hertz to megahertz in amorphous materials, in response to a strain wave of frequency ω, is widely thought to originate from the excitation of TLSs [22]. Mechanical energy from the wave ($V \pm \Delta/2$) can push the TLS to its saddle point. The TLS will then relax to state 2, transforming the mechanical energy into thermal energy. Dissipation from a given TLS will be maximized when its relaxation time [Eq. (2)] matches the inverse frequency of the dissipated excitation. An approximation for

relevant barriers is given by

$$V \sim k_B T \ln \frac{1}{\omega \tau_0}. \qquad (3)$$

In the context of gravitational wave detectors, mirrors are kept at temperatures ranging from room temperature down to cryogenic temperatures of 124 K [13]. At these temperatures and frequencies, quantum tunneling will be completely negligible in comparison to thermal activation, such that Eq. (1) is valid. Taking $\omega = 50$ Hz, we get relevant barriers of 0.28 and 0.67 eV for temperatures of 124 and 300 K, respectively.

If the entire distribution of the TLSs is known, the inverse quality factor, Q^{-1}, also called the loss angle of the bulk material, can be computed as follows:

$$Q_{(\omega)}^{-1} = \frac{1}{E} \sum_i \frac{\gamma_i^2}{k_B T} \frac{\omega \tau_i}{1 + \omega^2 \tau_i^2} \operatorname{sech}^2\left(\frac{\Delta_i}{2k_B T}\right). \qquad (4)$$

A detailed derivation for this equation can be found in Ref. [22]. The sum runs over every TLS in the system. τ_i and Δ_i are the relaxation time and asymmetry of the TLS i. E is the elastic modulus, and ω is the frequency of the applied strain. γ_i is the strength of the coupling between the TLS i and the strain called the deformation potential. This deformation potential can be obtained from the coupling tensor

$$\overline{\overline{\gamma}} = \partial \Delta / \partial \overline{\overline{\epsilon}}, \qquad (5)$$

where $\overline{\overline{\epsilon}}$ is the strain tensor.

Both γ and E depend on the nature of the strain. For example, to compute the attenuation of a longitudinal wave with Eq. (4), E will be the longitudinal modulus, and γ will be the longitudinal deformation potential. A detailed derivation was carried out by Damart and Rodney in Ref. [23].

B. Atomic models

To conduct this study, we consider quenched-melt and hyperuniform network models.

First, 200 quenched-melt systems of 1000 atoms of a-Si are generated. All 200 models are prepared using the molecular dynamics (MD) simulation software LAMMPS (large-scale atomic/molecular massively parallel simulator) [24] following the same melt-quench procedure: 1000 atoms are distributed randomly in a periodic box at a temperature of 3000 K, and the system is then cooled (quenched) at a (relatively) slow rate of 10^{11} K/s, freezing in an amorphous configuration. This method has the advantage of moderate computing cost and melt-quench methods with a slow cooling rate have been shown to generate samples that are in good agreement with well-annealed experimental a-Si [25,26].

We compare these models with a nearly hyperuniform network of a-Si developed by Hejna *et al.* [27]. This system was built using a modified version of the WWW algorithm [15] developed by Barkema and Mousseau [28]. The systems are then annealed for further relaxation and meticulously compared with experimental data.

While recent developments in machine-learning force fields [26] offer an interesting alternative to empirical potentials, the computational effort needed to generate a sufficient set of TLSs (more than 6 000 000 event searches), and

uncertainty as to the validity of these models regarding energy barriers associated with rare events, led us to turn to well-characterized empirical potentials. More specifically, a modified version of the Stillinger-Weber potential parameter set, developed by Vink *et al.* [29], was used and applied to the original formulation to simulate the structural and vibrational properties of *a*-Si.

For our topological analysis we define a cutoff value for two atoms to be connected at the middle point between the first and second peaks of the radial distribution function (Supplemental Fig. S1 [30]) for our configurations. This middle point lies around 3.05 Å. This cutoff definition and value are the same as those given in Ref. [28].

C. Activation-relaxation technique

In this paper we search for thermally activated events with characteristic times of the order of milliseconds to seconds. Here we elect to use activation-relaxation technique nouveau (ARTN) [31,32], a saddle-point search method that is ideally suited for such tasks as it focuses on finding high-barrier events (with high characteristic times) without having to compute every thermal atomic vibration.

This technique samples events in the potential energy landscape and finds their barriers and asymmetries. Characteristic times are then found using Eq. (2). MD-based methods can also be used to identify saddle points in such systems [23,33]. Because of the timescale on which such a method operates (nanoseconds), only low-energy barriers are efficiently identified. Those contribute to dissipation at low temperature or high frequency according to Eq. (3). Hence the two methods are complementary.

III. RESULTS AND DISCUSSION

A. Sampling

Using ARTN, we first explore the energy landscape around the final structure of the 200 quenched-melt 1000-atom configurations. For each sample, 30 ARTN searches are conducted per local topology. Since in amorphous materials the number of different environments is much larger than 1000, which is the number of local environments centered on the atoms in each of the systems, there are 30 000 event searches per configuration. While events with energy barriers ranging from 0 to a 5-eV cutoff are generated, only events with an activated barrier $0.2 \leqslant V \leqslant 0.7$ eV are considered in this paper because, as explained in Sec. II A, TLSs with lower or higher barriers will not contribute significantly to internal mechanical dissipation between the temperatures of 124 and 300 K [Eq. (3)]. A cutoff in asymmetry is chosen at $V = \Delta/3$, represented by the diagonal lines in Fig. 2, because the contribution to dissipation of events with higher asymmetry is exponentially suppressed by large Δ [see Eq. (4)]. Damart and Rodney have also shown in Ref. [23] that TLSs with larger asymmetry do not contribute to the mechanical loss. The barrier and asymmetry of the remaining events are plotted in Fig. 2. We note that the TLSs considered here represent only a very small fraction of all events found in this search.

TLS events found by ARTN can be characterized by the norm of the displacement of the main atom (i.e., the one
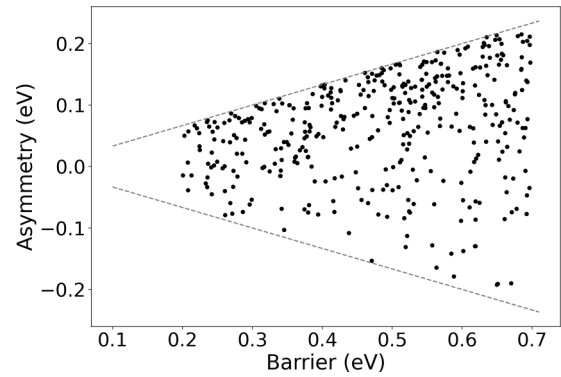

FIG. 2. Barrier and asymmetry of events found by ARTN. The gray dashed lines show the asymmetry cutoff.

moving the most) when the system transitions between two minima of the potential energy landscape and by the number of atoms involved in the transition. An atom is considered to be active if its displacement is greater than 0.1 Å.

Figure 3 shows the square root of the sum of squared displacements for active atoms; the marker color corresponds to the number of active atoms according to the scale on the right. We see that the magnitude of the atomic displacements is correlated with the energy barrier, although with considerable dispersion. In addition, a large displacement for the main atoms is generally associated with a larger number of active atoms (green dots). Conversely, the blue dots, representing events with a few active atoms, are at the bottom of the graph while the green dots, representing events with several active atoms, are at the top. In contrast, we have not found any correlation between local environment descriptors, such as bond-length or bond-angle distribution or Voronoi volume, and barriers. In general, TLS events involve between 5 and 30 active atoms, a number much smaller than the 20–150 active atoms found in oxide glasses [33,34]. This indicates that TLSs are much more localized phenomena in a more locally rigid structure with a higher coordination number, such as amorphous silicon, than oxides.
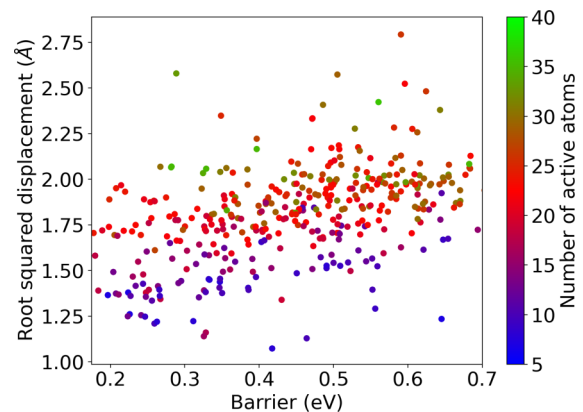

FIG. 3. Square root of squared atomic displacement in each TLS as a function of the energy barrier for the events plotted in Fig. 2. Symbols are color-coded according to the number of active atoms during the event (scale at right).
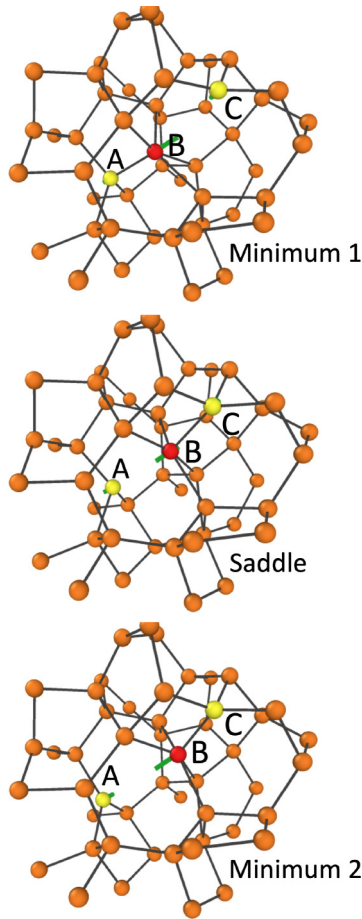
FIG. 4. Example of a bond-defect-hopping event (type 1) showing the system at both minima and at the saddle point. The central atom is in red. The atoms in yellow change their bonding status with the main atom. The green lines show the trajectory of the atoms between the frames.
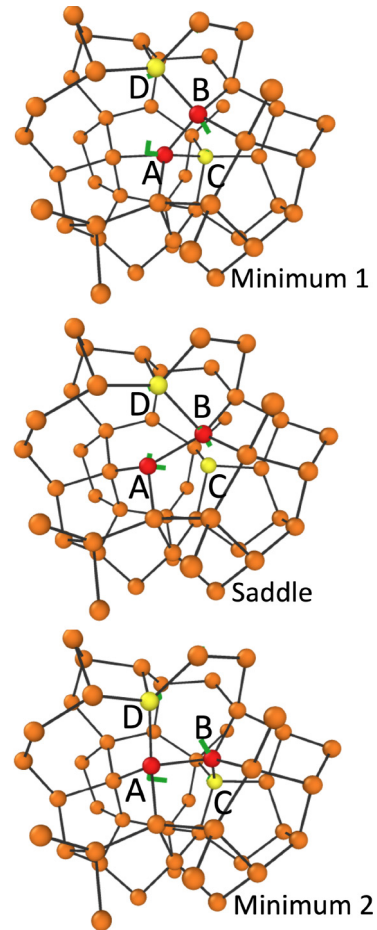

FIG. 5. Example of a bond-exchange TLS (type 2). The red atoms are the main atoms. The yellow atoms break a bond with one red atom and form a new bond with the other red atom. The green lines show the trajectory of the atoms between the frames.

B. Categorizing TLSs

Following the classification of activated events in *a*-Si developed by Barkema and Mousseau in Ref. [35], we adopt a three-class categorization based on the evolution of the bond network during events. The first category of TLSs (type 1) is associated with a bond hop from one atom to another. These events usually involve the diffusion of a coordination defect, such as dangling bond defects, and will be called *bond-defect-hopping TLSs*. These jumps are typically made possible by the movement of a single atom, leading to a relaxation of the surrounding environment.

In the example shown in Fig. 4, the main atom (atom B, in red) is fivefold coordinated. As for the yellow atoms, which are the ones that change their bond with the main atom during the process, atom A (in yellow) initially features fourfold coordination but becomes threefold coordinated at the end of the event. The inverse happens to atom C (also in yellow): It is initially threefold coordinated and becomes fourfold coordinated during the process.

The second category of TLSs (type 2) corresponds to the (WWW) bond-exchange mechanism [15], and TLSs in this category are called *bond-exchange TLSs*. This mechanism is commonly observed in *a*-Si [20,35] and has been described in other amorphous and crystalline solids such as graphene [36]. It involves two connected atoms exchanging their respective bonds between them. An example is provided in Fig. 5. Atoms A and B (in red) stay connected at all times and exchange their bonds with atoms C and D (in yellow). Interestingly, these events do not depend on the presence of a bond defect to occur, as opposed to type 1 events, and can occur in a material featuring few voids.

The third class of events includes all TLSs that do not fit the first or the second category. Typically, these TLSs involve three or more atoms. While it is formally possible to further analyze them [20,37], their diversity limits the understanding we can gain from their detailed classification, so we will focus on type 1 and 2 TLSs.

Figure 6 shows that bond-defect-hopping and bond-exchange TLSs exhibit different barrier distributions. Bond-defect-hopping TLSs are associated with lower barriers than bond-exchange TLSs, due to the presence of a bonding defect on the central atoms. The strain associated with these defects increases the potential energy of the two minima and lowers the saddle-point barrier. Asymmetries, on the other hand, are distributed relatively evenly for all types of TLSs.
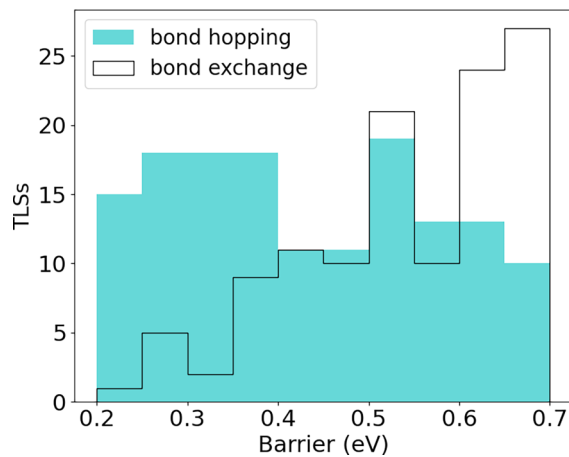
FIG. 6. Barrier distribution of bond-defect -hopping (cyan bars) and bond-exchange TLSs (bars outlined in black).

C. Mean trends

Local environments that support TLSs display some structural characteristics that separate them from the rest of the sample.

These can be summarized by looking at the local density obtained from computing the Voronoi volume surrounding each atom. While the average density, as measured over all atoms, is 2.20 g/cm^3, the local value surrounding the dominant atom associated with TLSs is only 2.08 g/cm^3. These zones of low density are associated with strained or under-coordinated atoms, creating local instabilities that favor the formation of TLSs. Figure 7 confirms this by showing that the dominant atom associated with TLSs has a longer bond (top graph, dashed and dash-dotted curves) and a wider bond-angle distribution (bottom graph, dashed and dash-dotted curves) compared with all the atoms of the system (black solid curves).

D. Relation between structure and mechanical loss

Experiments have shown that thermal annealing or deposition at high substrate temperature reduces significantly the mechanical loss of amorphous materials [38], especially silicon [14]. It is generally argued that this reduction is due to thermal activation that allows the material to reach more relaxed states.

To assess the importance of this effect here, we compare configurations obtained by different means. More specifically,
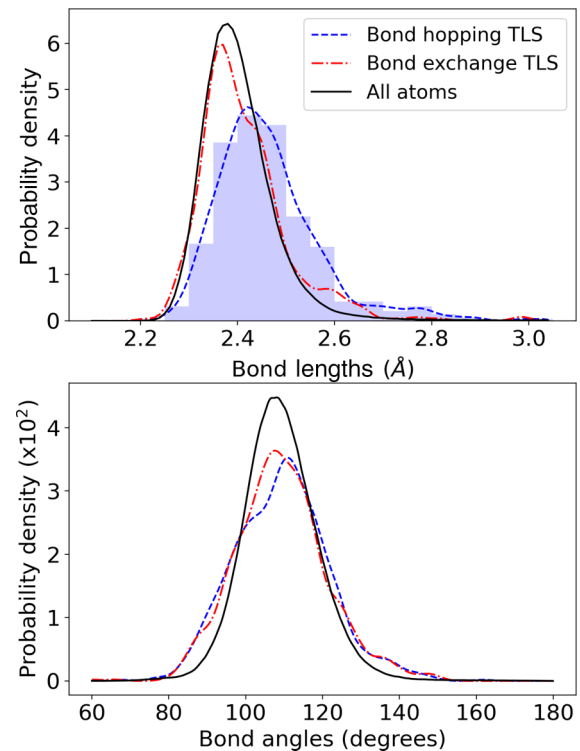

FIG. 7. Smoothed distribution of the bond lengths (top) and the bond angles (bottom) of the main active atom in the bond-defect-hopping (blue dashed curves) and bond-exchange TLSs (red dash-dotted curves). The black solid curves represent the first peak and bond-angle distribution of the RDF of our *a*-Si configurations. A raw histogram (blue, top) is also shown to illustrate the effect of the smoothing.

we compare the systems discussed until now, obtained by melt-quench models, with a nearly hyperuniform network (NHN) model built by Hejna *et al.* [27] and presented in Sec. II B.

We present some physical and structural characteristics of samples prepared using the two methods in Table I. Despite similar atomic densities and potential energy per atom, the configuration obtained with a bond-exchange approach shows a significantly lower density of point defects compared with that obtained with a melt-quench approach.

The lower density of the NHN configuration is reflected in its TLS distribution generated with ARTN, as before. Figure 8 shows a depleted TLS distribution in the NHN configura-

TABLE I. Characteristics of *a*-Si configurations prepared by melt quench (this paper) and by bond exhange (NHN) [15,27]. Uncertainties in the melt-quench column correspond to the standard deviation computed over 200 independent samples. *N*, number of defects or TLSs.

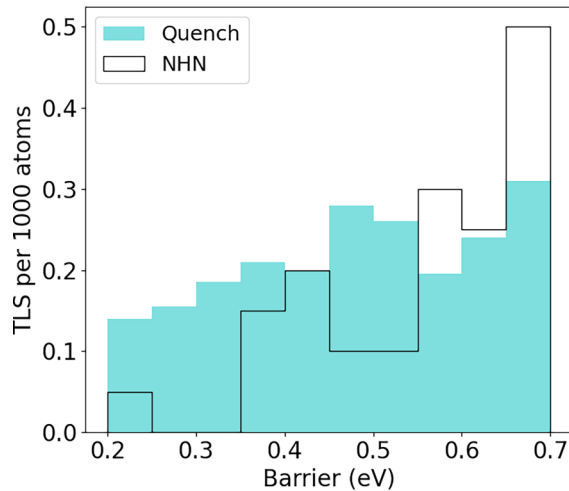| Sample	Melt quench	Bond exchange (NHN)
Energy (eV per atom)	-3.078 ± 0.004	-3.089
Density (g/cm^3)	2.200 ± 0.006	2.21
Overcoordination defects (*N* per 1000 atoms)	17 ± 4	0.4
Undercoordination defects (*N* per 1000 atoms)	7 ± 2	0.45
TLSs found, nominal (*N*)	390	33
TLSs found (*N* per 1000 atoms)	1.95	1.65

FIG. 8. Energy barrier distribution for the TLSs in models obtained by the melt-quench and NHN preparation methods (described in the text).

FIG. 10. Internal mechanical dissipation computed for quenched *a*-Si (black) and NHN *a*-Si (red). The pale curves show the contributions from individual TLSs. Blue circles and blue diamonds are experimental data in *a*-Si deposited at 45 and 200 °C, respectively, from Ref. [14].

tion at low barriers (between 0.1 and 0.4 eV) as compared with the melt-quench models. This depletion is associated with a reduced ratio of bond-defect-hopping TLSs (type 1) to bond-exchange (type 2) TLSs. This is not too surprising considering that bond-hopping events have in general lower barriers (Fig. 6) and often involve coordination defects, which are much rarer in the NHN model as seen from Table I. Figure 9 shows histograms of the number of events by type in the melt-quench and NHN models normalized by the number of atoms in each model. This not only confirms the much lower density of bond-defect-hopping events in NHN models but also underlines that the similar strain leads to a roughly similar total density of TLSs on both the NHN and the melt-quenched systems (see also Table I).

E. Loss angle calculations

Knowing the microscopic details of TLSs, it is possible to compute directly the mechanical loss of *a*-Si using Eq. (4). The details and approximations used are described in Sec. II A.
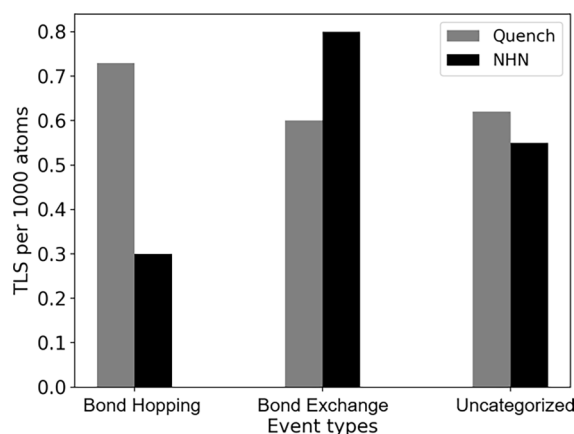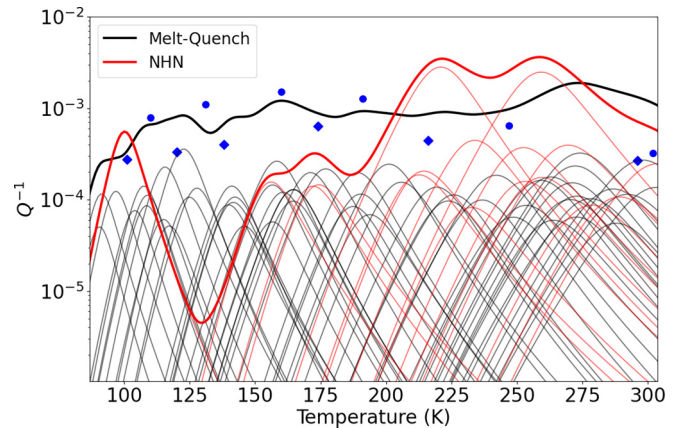

FIG. 9. Density of the three types of TLSs in quenched *a*-Si (gray) and NHN *a*-Si (black).

The first step is to compute the strain-asymmetry coupling tensor in Eq. (5). We obtain this quantity by applying a small affine deformation to both minima of every TLS. The potential energy of each minimum is then computed. This is done for both positive and negative strain, and results are averaged over both. We verify that varying the amplitude of the deformation does not change the results.

The deformation potentials for longitudinal and traverse strain waves are then computed using the formula derived by Damart and Rodney [23]. For the longitudinal deformation potentials, we get values between 0.5 and 9.1 eV and a mean value of 4.1 eV, and for the transverse case we get energies ranging from 0.4 to 7.8 eV with a mean value of 3.4 eV. Deformation potentials are found to be uncorrelated with the barrier or the asymmetry. Experiments have reported average transverse deformation potentials of 1 eV [39]; however, those experiments were conducted below 1 K, and so barriers involved were much lower than those studied in this paper. So we suppose the minima of active TLSs to be closer in geometry and their deformation potential to be lower.

Mechanical loss predictions are presented in Fig. 10 for both the melt-quench (black) and NHN configurations (red). The thin curves represent each term in the sum [Eq. (4)], while the thick curve is the total. The melt-quench configurations lead to an almost constant Q^{-1} value close to 10^{-3} at temperatures between 100 and 300 K. This compares well with experimental measurements on *a*-Si deposited at 45 and 200 °C that show Q^{-1} values between 10^{-4} and 10^{-3} [14]. In particular, the loss angle in our melt-quenched systems is very close to the experimental loss angle in *a*-Si deposited at 45 °C. This difference is expected because the short cooling time of our simulations is equivalent to a low deposition temperature in the sense that both leave little time for relaxation events to take place.

Because we consider only one sample, the NHN system presents a much lower absolute number of TLSs (33 vs 390), leading to more noise: A few TLSs are causing peaks in the dissipation for this system, namely, the ones centered at 100, 225, and 260 K. These TLSs have such high contribu-

tions because of their very low asymmetry (0.009, 0.021, and 0.034 eV, respectively). We expect that these peaks would flatten with more data obtained for a larger system or better statistics.

Nevertheless, it is remarkable that the NHN configuration yields a similar mechanical loss to that of the melt-quench around room temperature. Dropping down to cryogenic temperatures, however, the mechanical loss decreases significantly, getting as low as 10^{-5} (although this result is strongly influenced by single TLSs, such as the one producing a peak near 100 K). In the previous section we showed that the bond-defect-hopping TLSs, which compose most of the low-barrier TLSs in a-Si (Fig. 9), are much less frequent in the NHN configuration, causing the rarefaction of low barriers in this configuration (Fig. 8). The same explanation applies here as well, as low barriers are active at these low temperatures. Despite the smaller sample size of the NHN causing sharp peaks in the mechanical loss calculations, the reduction in the number of low-barrier TLSs is very clear (Table I); therefore this decrease in the loss angle with temperature should be significant.

This behavior of Q^{-1} in the NHN a-Si is similar to that of experimental hydrogenated a-Si, where the mechanical loss is high at room temperature but decreases significantly between 300 and 10 K [40]. We validate this calculation, made on TLSs selected in Sec. II A for consistency, by comparing it with the the Q^{-1} computation over all events found with barriers less than 1.2 eV and find that the results do not change (see Supplemental Fig. S2) [30].

IV. SUMMARY AND CONCLUSION

This study aims to identify the structural origin of internal mechanical dissipation in amorphous solids. To do so, we focus on a-Si, a classical reference for covalent disordered materials. More precisely, we characterize the two-level systems (TLSs) found in 200 sets of 1000 atoms of melt-quench-generated configurations and a single nearly hyperuniform network (NHN) of 20 000 atoms built by Hejna, Steinhardt, and Torquato [27] using the WWW algorithm. Both configurations feature similar energies per atoms; however, melt-quench-generated a-Si has around 2.5% topological defects (threefold and fivefold coordinated atoms), while the NHN shows almost none. The potential energy landscape is explored with ARTN [31,32]. We keep only TLSs with small barriers (0.2–0.7 eV) and asymmetries ($< V/3$) because they correspond to the experimental observation window. There are 390 TLSs in the melt-quench a-Si and 33 in the NHN that are considered relevant to our study and further analyzed.

Loss angle calculations on these systems lead to a high loss angle close to 10^{-3} for both NHN and melt-quench a-Si at room temperature. While the loss angle in the melt-quench configurations stays relatively constant with temperature, NHN a-Si shows an important decrease in loss angle when the temperature drops from 300 to 100 K, a similar behavior to that observed experimentally in well-relaxed a-Si [14].

With the detailed information obtained through ARTN, TLSs can be classified by the bond-network change associated with the two-level system. Two-thirds of events fall into two categories: bond-defect hopping and bond exchange. These

two types of TLSs are associated with different local configurations: Bond-defect hopping happens around coordination defects and where bonds are stretched, and bond-exchange TLSs are found in regions where all atoms are fourfold coordinated but present small angle defects.

Our simulations demonstrate that various classes of TLSs can occur with different concentrations according to the preparation schedule. Quenching from a melt results in bond-defect hopping being the dominant TLS type, because of the high concentration of trapped point defects in these configurations. The NHN of a-Si has next to no point defects. This drastically reduces the concentration of bond-hopping TLSs but has little effect on the concentration of bond-exchange TLSs. From this we learn that TLSs are independent: The presence of one type of TLSs does not depend on the existence of other types. We also show that the types of TLSs we find in different configurations are specific to the preparation, or the relaxation path, of said configuration.

Investigating other systems is necessary to improve our understanding of the atomistic origin of TLSs and internal mechanical dissipation. Work on oxide glasses was done in Refs. [23,33,34]. In Ref. [23], Damart and Rodney analyzed TLSs in SiO_2 and found archetypes of TLSs that are different from those found in a-Si, such as rotations of Si-O-Si chains. This suggests that TLSs are also specific to the nature of the material, for instance, between a-Si and oxide glasses such as SiO_2 and Ta_2O_5.

This work aims to provide insight into the reduction of thermal noise (and at the same time mechanical loss) in the mirrors of GWDs. Here, we find that decreasing TLSs in amorphous materials means not only understanding the nature of events for specific systems but also addressing separately each of the potential classes of TLSs. Our results suggest that reduction of mechanical loss in GWDs will necessitate the suppression of each different type of TLS. In the case of a-Si, this means directly addressing two well-defined major categories of TLSs and a collection of more diverse, uncategorized TLSs that make up about a third of all TLSs, all of which may require different strategies to eliminate, once overall strain reduction become impossible.

Because of the importance of specificity, further study would benefit from better physical description to ensure that the atomistic details of TLSs are accurate. Since larger amorphous configurations tend to better reproduce experimental observations [28,41], *ab initio* approaches are probably not appropriate. Recent developments in machine-learning force fields [26] offer here a new opportunity to deepen our understanding of these fascinating problems, as we better understand their validity for describing the rare events associated with TLSs.

The ARTN packages as well as the data reported here are distributed freely. Please contact N. Mousseau.

[1] R. Abbott, T. D. Abbott, F. Acernese, K. Ackley, C. Adams, N. Adhikari, R. X. Adhikari, V. B. Adya, C. Affeldt, D. Agarwal, O. D. Aguiar, L. Aiello, A. Ain, P. Ajith, B. Allen, A. Allocca, P. A. Altin, S. B. Anderson, W. G. Anderson, K. Arai *et al.* (LIGO Scientific Collaboration and Virgo Collaboration), Phys. Rev. Lett. **116**, 061102 (2016).

[2] R. Abbott, T. D. Abbott, F. Acernese, K. Ackley, C. Adams, N. Adhikari, R. X. Adhikari, V. B. Adya, C. Affeldt, D. Agarwal, M. Agathos, K. Agatsuma, N. Aggarwal, O. D. Aguiar, L. Aiello, A. Ain, P. Ajith, S. Akcay, T. Akutsu, S. Albanesi *et al.* (LIGO Scientific Collaboration, Virgo Collaboration, and KAGRA Collaboration), arXiv:2111.03606.

[3] G. M. Harry, M. R. Abernathy, A. E. Becerra-Toledo, H. Armandula, E. Black, K. Dooley, M. Eichenfield, C. Nwabugwu, A. Villar, D. R. M. Crooks, G. Cagnoli, J. Hough, C. R. How, I. MacLaren, P. Murray, S. Reid, S. Rowan, P. H. Sneddon, M. M. Fejer, R. Route *et al.*, Classical Quantum Gravity **24**, 405 (2007).

[4] R. Kubo, Rep. Prog. Phys. **29**, 255 (1966).

[5] P. R. Saulson, Phys. Rev. D **42**, 2437 (1990).

[6] Y. Levin, Phys. Rev. D **57**, 659 (1998).

[7] G. M. Palma, K.-A. Suominen, and A. K. Ekert, Proc. R. Soc. London Ser. A **452**, 567 (1996).

[8] M. Abernathy, A. Amato, A. Ananyeva, S. Angelova, B. Baloukas, R. Bassiri, G. Billingsley, R. Birney, G. Cagnoli, M. Canepa, M. Coulon, J. Degallaix, A. D. Michele, M. A. Fazio, M. M. Fejer, D. Forest, C. Gier, M. Granata, A. M. Gretarsson, E. M. Gretarsson *et al.*, Classical Quantum Gravity **38**, 195021 (2021).

[9] M. Granata, A. Amato, G. Cagnoli, M. Coulon, J. Degallaix, D. Forest, L. Mereni, C. Michel, L. Pinard, B. Sassolas, and J. Teillon, Appl. Opt. **59**, A229 (2020).

[10] E. Lalande, A. W. Lussier, C. Lévesque, M. Ward, B. Baloukas, L. Martinu, G. Vajente, G. Billingsley, A. Ananyeva, R. Bassiri, M. M. Fejer, and F. Schiettekatte, J. Vac. Sci. Technol. A **39**, 043416 (2021).

[11] R. Nawrodt, S. Rowan, J. Hough, M. Punturo, F. Ricci, and J.-Y. Vinet, Gen. Relativ. Gravitation **43**, 593 (2011).

[12] L. J. Lewis, J. Non-Cryst. Solids **580**, 121383 (2022).

[13] R. Birney, J. Steinlechner, Z. Tornasi, S. MacFoy, D. Vine, A. S. Bell, D. Gibson, J. Hough, S. Rowan, P. Sortais, S. Sproules, S. Tait, I. W. Martin, and S. Reid, Phys. Rev. Lett. **121**, 191101 (2018).

[14] X. Liu, D. R. Queen, T. H. Metcalf, J. E. Karel, and F. Hellman, Phys. Rev. Lett. **113**, 025503 (2014).

[15] F. Wooten, K. Winer, and D. Weaire, Phys. Rev. Lett. **54**, 1392 (1985).

[16] D. Wales, *Energy Landscapes: Applications to Clusters, Biomolecules and Glasses*, Cambridge Molecular Science (Cambridge University Press, Cambridge, 2004).

[17] P. W. Anderson, B. I. Halperin, and c. M. Varma, Philos. Mag. **25**, 1 (1972).

[18] H. Kallel, N. Mousseau, and F. Schiettekatte, Phys. Rev. Lett. **105**, 045503 (2010).

[19] S. Gelin, A. Champagne-Ruel, and N. Mousseau, Nat. Commun. **11**, 3977 (2020).

[20] F. Valiquette and N. Mousseau, Phys. Rev. B **68**, 125209 (2003).

[21] J. Jäckle, L. Piché, W. Arnold, and S. Hunklinger, J. Non-Cryst. Solids **20**, 365 (1976).

[22] W. A. Phillips, Rep. Prog. Phys. **50**, 1657 (1987).

[23] T. Damart and D. Rodney, Phys. Rev. B **97**, 014201 (2018).

[24] A. P. Thompson, H. M. Aktulga, R. Berger, D. S. Bolintineanu, W. M. Brown, P. S. Crozier, P. J. in 't Veld, A. Kohlmeyer, S. G. Moore, T. D. Nguyen, R. Shan, M. J. Stevens, J. Tranchida, C. Trott, and S. J. Plimpton, Comput. Phys. Commun. **271**, 108171 (2022).

[25] M. Ishimaru, S. Munetoh, and T. Motooka, Phys. Rev. B **56**, 15133 (1997).

[26] V. L. Deringer, N. Bernstein, A. P. Bartók, M. J. Cliffe, R. N. Kerber, L. E. Marbella, C. P. Grey, S. R. Elliott, and G. Csányi, J. Phys. Chem. Lett. **9**, 2879 (2018).

[27] M. Hejna, P. J. Steinhardt, and S. Torquato, Phys. Rev. B **87**, 245204 (2013).

[28] G. T. Barkema and N. Mousseau, Phys. Rev. B **62**, 4985 (2000).

[29] R. L. C. Vink, G. T. Barkema, W. F. van der Weg, and N. Mousseau, J. Non-Cryst. Solids **282**, 248 (2001).

[30] See Supplemental Material at http://link.aps.org/supplemental/10.1103/PhysRevMaterials.6.123604 for the additional figures.

[31] G. T. Barkema and N. Mousseau, Phys. Rev. Lett. **77**, 4358 (1996).

[32] R. Malek and N. Mousseau, Phys. Rev. E **62**, 7723 (2000).

[33] R. Hamdan, J. P. Trinastic, and H. P. Cheng, J. Chem. Phys. **141**, 054501 (2014).

[34] J. P. Trinastic, R. Hamdan, C. Billman, and H.-P. Cheng, Phys. Rev. B **93**, 014105 (2016).

[35] G. T. Barkema and N. Mousseau, Phys. Rev. Lett. **81**, 1865 (1998).

[36] A. Stone and D. Wales, Chem. Phys. Lett. **128**, 501 (1986).

[37] N. Mousseau and G. T. Barkema, Phys. Rev. B **61**, 1898 (2000).

[38] G. Vajente, R. Birney, A. Ananyeva, S. Angelova, R. Asselin, B. Baloukas, R. Bassiri, G. Billingsley, M. M. Fejer, D. Gibson, L. J. Godbout, E. Gustafson, A. Heptonstall, J. Hough, S. MacFoy, A. Markosyan, I. W. Martin, L. Martinu, P. G. Murray, S. Penn *et al.*, Classical Quantum Gravity **35**, 075001 (2018).

[39] A. Fefferman, A. Maldonado, E. Collin, X. Liu, T. Metcalf, and G. Jernigan, J. Low Temp. Phys. **187**, 654 (2017).

[40] X. Liu, B. E. White, Jr., R. O. Pohl, E. Iwanizcko, K. M. Jones, A. H. Mahan, B. N. Nelson, R. S. Crandall, and S. Veprek, Phys. Rev. Lett. **78**, 4418 (1997).

[41] D. Igram, B. Bhattarai, P. Biswas, and D. A. Drabold, J. Non-Cryst. Solids **492**, 27 (2018).